https://doi.org/10.15407/ujpe69.6.417

I.I. YAKOVKIN, M.F. LEDNEY

Taras Shevchenko National University of Kyiv, Faculty of Physics
(60 Volodymyrs'ka Str., Kyiv 01601, Ukraine; e-mail: yakovkinii@gmail.com)

ELECTROCONTROL OVER SURFACE PLASMON OSCILLATIONS IN A HOMEOTROPIC NEMATIC LIQUID CRYSTAL CELL

The electric-field-induced orientational instability of the director in a cell of homeotropically oriented nematic liquid crystal (NLC) in the presence of a pretilt of the director on the substrate surface has been theoretically studied. It is found that the orientational transitions of the NLC director field from the initial homogeneous state to a significantly inhomogeneous one and the following transition into the planar state are induced by changes in the electric field strength and can be accompanied by hysteresis phenomena. The parameters of the latter are calculated, and conditions required for the hysteresis phenomena to exist, as well as their dependences on the NLC cell parameters, are determined. It is found that an increasing in the director pretilt at the substrate and/or the anchoring energy of the NLC with the inclined easy axis makes the hysteresis loop narrower, which may lead to the hysteresis disappearance in those orientational transitions. The propagation of the surface plasmon polariton (SPP) along the NLC cell surface in the case where one of the cell's polymer substrates is covered on the outer side with a gold layer has also been investigated. The magnitude of the effective refractive index for the SPP is calculated, and it is found that its value decreases as the electric field strength increases. It is also found that the range of control over the SPP effective refractive index expands for smaller values of the tilt angle of the inclined easy axis and the polymer layer thickness, as well as for larger values of the SPP wavelength and the NLC optical anisotropy.

K e y w o r d s: nematic liquid crystal, orientational instability, hysteresis of orientational transition, director pretilt, anchoring energy, surface plasmon polariton.

1. Introduction

Intensive scientific research performed in the field of liquid crystal physics during the last decades has led to the wide practical application of liquid crystals in physics, medicine, and industry [1, 2]. The use of cells of liquid crystals – in particular, nematic liquid crystals (NLCs) – as an element basis for electronic-optical devices of various types is associated with the relative cheapness of NLCs and their unique electro- and magneto-optical properties. The latter are closely related to the orientational ordering of molecules in the NLC mesophase, which substantially depends on the conditions for the director at the confining cell surface [7–9].

Owing to the interaction of NLC molecules with one another, their interaction with the cell surface spreads into the bulk, thus creating a certain orientational ordering there [10–14]. This ordering can be controlled relatively easily by applying external fields (electric, magnetic, or electromagnetic) [15–20]. As a result, it becomes possible to vary the optical properties of the whole bulk specimen in a controllable way. This circumstance makes NLC systems a promising tool for the effective and easy control over the propagation and transmission of electromagnetic signals. In particular, modern laboratory and technological applications have already demonstrated a possibility to effectively tune the optical and spectral properties of photonic crystals [21,22] and waveg-

C i t a t i o n: Yakovkin I.I., Ledney M.F. Electrocontrol over surface plasmon oscillations in a homeotropic nematic liquid crystal cell. *Ukr. J. Phys.* **69**, No. 6, 417 (2024). https://doi.org/10.15407/ujpe69.6.417.

Ц и т у в а н н я: Яковкін І.І., Ледней М.Ф. Електрокерування поверхневими плазмонними коливаннями в гомеотропній комірці нематичного рідкого кристала. *Укр. фіз. журн.* **69**, №6, 417 (2024).

uides [23], as well as other applications where NLC layers are used as control elements. In a number of practical applications, NLCs on the confining surfaces of cells often create conditions for a director pretilt to appear [24, 25]. The director pretilt reduces the probability of formation of non-planar deformations and defects in the NLC bulk [26–28], and also provides a smoother control over the optical properties of the system with the help of external fields.

Note that electrically induced orientational transitions in NLC cells with the director pretilt at the cell surface were often considered analytically. However, it was done in the constant electric field approximation. In this approximation, it is assumed that the director distribution in the cell does not affect the magnitude of the electric field in the NLC bulk. This considerably simplifies the analysis and allows both the stationary director states and the reorientation dynamics to be studied analytically. For instance, in work [29], the orientational transitions in an NLC cell with the director pretilt at the surface from a planar state to a homeotropic one in a constant electric field directed perpendicular to the cell surface were considered using the indicated method. The influence of a pretilt angle and the anchoring energy on the orientational director instability in a homeotropic NLC cell with negative dielectric anisotropy when a potential difference is applied to the cell substrates was studied in works [30–32].

Orientational transitions induced in a system by an external field can be accompanied by hysteresis phenomena, which manifest themselves as the bistability [33–36] and multistability [37, 38] of the director field. Such features of the orientational reconstruction of the NLC can reveal themselves in both the light [39, 40] and constant [41] electric field (in the latter case, if the field is mostly oriented along the surface of the substrates). Such a behavior expands the application prospects of NLC systems on the way to creating highly efficient bistable displays, optical shutters, and so forth. The study of such fine effects as the possibility of bistable states in the system requires that the influence of the director orientation on both the amplitude and the direction of the local electric field vector in the NLC bulk has to be taken into account. As a result, the equations for the director must be solved in coordination with the electrodynamic equations for the electric or light field. The general theoretical foundations of such approach were outlined in works [42] and [43] for Fréedericksz transitions in stationary electric and light fields, respectively.

Widely known is the application of NLCs to control the characteristics of plasmonic structures [44–48]. In particular, under certain conditions, surface plasmon polaritons (SPPs) can be excited at the metal–polymer interface. The enhanced sensitivity of SPPs to small changes in the dielectric constant of the medium, on the one hand, and a high NLC sensitivity to the influence of external fields, on the other hand, found a successful combination in the three-layer system NLC–polymer layer–metal. This structure makes it possible to control the SPP propagation characteristics, in particular, the value of the SPP effective refractive index, by varying the orientation of the NLC director using an external field [49–52]. The possibility to tune the SPP propagation characteristics using NLCs opened a way to create spatial light modulators [53, 54], spectral filters [55–57], light intensity modulators [58, 59], gratings with controlled transmittance [60], and so on.

In this work, we theoretically study the orientational instability of the director field in a homeotropic NLC cell with the director pretilt at the surface in an external electric field. It is found that the orientational director transitions from an initial homogeneous state to a non-homogeneous one and vice versa, as well as from a non-homogeneous state to the planar one and vice versa, induced by changing the electric field strength can be accompanied by a hysteresis. The hysteresis parameters of the indicated orientational transitions are calculated, and the conditions for their occurrence, as well as their dependence on system parameters, were determined. The SPP propagation at the surface of the polymer substrate that confines the NLC was considered, provided that a thin layer of gold covers the other side of the substrate. The value of the SPP effective refractive index and its dependence on the electric field strength, the thickness of the polymer substrate, and the angle of the easy orientation axis of the director at the substrate surface are calculated.

2. Stationary Distributions of the Director Field

Let us have a plane-parallel NLC cell confined between the planes $z = 0$ and $z = L$. The initial orientation of the director is mostly homeotropic and uniform, and it is determined by the two axes, **e** and

ν, of the light orientation of the director at the surface [61,62]. The **e**-axis defines the homeotropic (normally to the surface) orientation of the director, and the ν-axis defines the oblique orientation of the director. The cell is in a constant and uniform electric field with the strength vector $\mathbf{E}_0$, which is oriented along the cell surface in the plane of the axes **e** and ν (see Fig. 1).

The free energy of the NLC cell is written in the form

$$F = F_{\rm el} + F_E + F_S, \tag{1}$$

where

$$F_{\rm el} = \frac{1}{2}\int\limits_V \Big\{K_1(\operatorname{div}\mathbf{n})^2 + K_2(\mathbf{n}\cdot\operatorname{rot}\mathbf{n})^2 + K_3[\mathbf{n}\times\operatorname{rot}\mathbf{n}]^2\Big\}\,dV$$

is the elastic energy of the NLC;

$$F_E = -\frac{1}{8\pi}\int\limits_V \mathbf{E}\hat{\epsilon}\mathbf{E}\,dV$$

is the anisotropic contribution of the NLC interaction with the electric field to the free energy;

$$F_S = -\frac{W_e}{2}\int\limits_{S_{1,2}} (\mathbf{en})^2\,dS - \frac{W_\nu}{2}\int\limits_{S_{1,2}} (\nu\mathbf{n})^2\,dS$$

is the surface free energy of the NLC; K_1, K_2, and K_3 are elastic constants; **n** is the NLC director; **E** is the electric field strength vector in the NLC bulk; $\hat{\epsilon} = \epsilon_\perp\hat{\mathbf{l}} + \epsilon_a\mathbf{n}\otimes\mathbf{n}$ and $\epsilon_a = \epsilon_\parallel - \epsilon_\perp > 0$ are the tensor and anisotropy, respectively, of the static NLC permittivity; and W_e and W_ν are the anchoring energies of the director with its easy orientation axes **e** and ν, respectively, at the cell surfaces. Note that in the formula for the surface free energy F_S, we restricted the consideration to the simple but the most often used Rapini model [63] with two axes, **e** and ν, of the easy director orientation [61, 62] at the confining cell surfaces.

Let us consider plane deformations of the NLC director field that lie in the plane xOz. The latter coincides with the plane containing the **e**- and ν-axes and the vector $\mathbf{E}_0$. Due to the system homogeneity along the axis Oy, the director **n** in the NLC bulk can be written in the form

$$\mathbf{n} = \mathbf{i}\cdot\sin\theta(z) + \mathbf{k}\cdot\cos\theta(z), \tag{2}$$

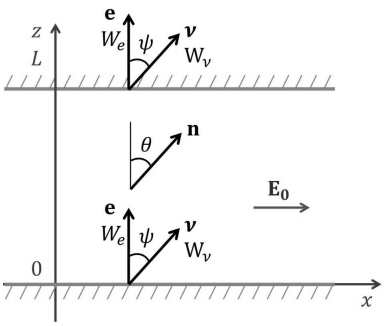

Fig. 1. Geometry of the problem

where **i** and **k** are the unit vectors of the Cartesian coordinate system, and θ is the director deviation angle from the Oz-axis.

The equilibrium distributions of the director field correspond to the stationary points of the free energy functional F [Eq. (1)]. To find them, the variational equations for the director **n** must be solved together with the equations for the electric field **E** in the NLC bulk. Assuming the system under consideration to be homogeneous along the Ox-axis, the electric field strength vector in the NLC bulk can be written in the form $\mathbf{E} = \big(E_x(z), 0, E_z(z)\big)$. From the equation $\operatorname{rot}\mathbf{E} = 0$, it follows that the component E_x of the vector **E** does not depend on the coordinate z. Using the electrostatic boundary conditions, the indicated component takes the form $E_x = E_0$.

From the equation $\operatorname{div}\mathbf{D} = 0$, it follows that the component D_z of the electric field induction vector is constant and equals zero according to the electrostatic boundary conditions. From this condition, we find the component $E_z = -\epsilon_{xz}E_0/\epsilon_{zz}$ of the electric field strength vector **E**. Taking into account the aforesaid, the free energy functional F [Eq. (1)] can be written in the form

$$F = \frac{1}{2}\int\limits_0^L \big(K_1\sin^2\theta + K_3\cos^2\theta\big)\theta_z'^2\,dz - \frac{\epsilon_\parallel\epsilon_\perp E_0^2}{8\pi}\int\limits_0^L \frac{dz}{\epsilon_\perp + \epsilon_a\cos^2\theta} - \frac{W_e}{2}\big(\cos^2\theta_0 + \cos^2\theta_L\big) - \frac{W_\nu}{2}\big(\cos^2(\theta_0-\psi) + \cos^2(\theta_L-\psi)\big), \tag{3}$$

where $\theta_0 = \theta(z=0)$ and $\theta_L = \theta(z=L)$ are the director orientation angles at the lower and upper,

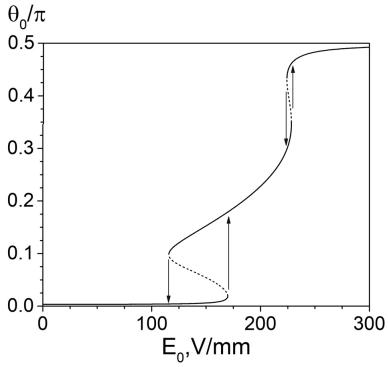

Fig. 2. Dependence of the director angle θ_0 at the surface ($z = 0$) on the electric field strength E_0. The solid curves correspond to stable solutions, and the dashed curves to unstable ones. The arrows mark orientational transitions in the system

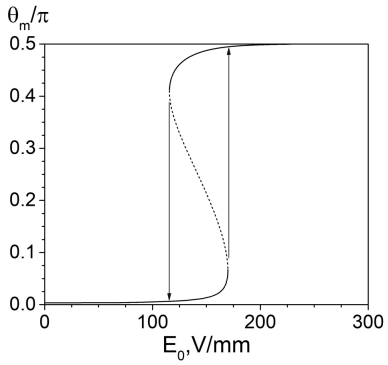

Fig. 3. Dependence of the maximum director angle θ_m on the electric field strength E_0. The solid curves correspond to stable solutions, and the dashed curves to unstable ones. The arrows mark orientational transitions in the system

respectively, cell surfaces; and ψ is the deviation angle of the axis ν from the direction Oz; hereafter, the primed θ denotes the derivatives of θ with respect to the coordinate z.

The minimization of functional (3) in the angle θ brings about the equation

$$\frac{1}{2}(K_1 - K_3)\sin 2\theta\,\theta_z^{'\,2} + (K_1\sin^2\theta + K_3\cos^2\theta)\,\theta_{zz}^{''} + \\ + \frac{\epsilon_\parallel\epsilon_\perp\epsilon_a E_0^2}{4\pi}\frac{\sin\theta\cos\theta}{(\epsilon_\perp + \epsilon_a\cos^2\theta)^2} = 0, \tag{4}$$

and the boundary conditions

$$\begin{aligned}&\left[-2(K_1\sin^2\theta + K_3\cos^2\theta)\,\theta_z^{'} + W_e\sin 2\theta + \right.\\ &\left. + W_\nu\sin 2(\theta - \psi)\right]_{z=0} = 0,\\ &\left[2(K_1\sin^2\theta + K_3\cos^2\theta)\,\theta_z^{'} + W_e\sin 2\theta + \right.\\ &\left. + W_\nu\sin 2(\theta - \psi)\right]_{z=L} = 0.\end{aligned} \tag{5}$$

Owing to the problem symmetry with respect to the coordinate transformation $z \to L - z$, the stationary director distributions must satisfy the condition $\theta(z) = \theta(L - z)$. Then, either of boundary conditions (5) can be replaced by the condition $\theta'(z = L/2) = 0$ or the equivalent condition $\theta(z = L/2) = \theta_m$, where θ_m is the maximum value of the director angle. By integrating Eq. (4) twice over the variable z and, in view of boundary conditions (5), we obtain the following equation for determining the dependence $\theta(z)$:

$$z = \frac{1}{E_0}\sqrt{\frac{4\pi\,(\epsilon_\perp + \epsilon_a\cos^2\theta_m)}{\epsilon_\parallel\epsilon_\perp\epsilon_a}}\times \\ \times\int\limits_{\theta_0}^{\theta}\sqrt{\frac{(K_1\sin^2\theta + K_3\cos^2\theta)(\epsilon_\perp + \epsilon_a\cos^2\theta)}{\cos^2\theta - \cos^2\theta_m}}\,d\theta, \tag{6}$$

where the director orientation angle θ_0 at the surface $z = 0$ and the maximum angle θ_m of the director are determined from the system of equations

$$\frac{L}{2} = \frac{1}{E_0}\sqrt{\frac{4\pi\,(\epsilon_\perp + \epsilon_a\cos^2\theta_m)}{\epsilon_\parallel\epsilon_\perp\epsilon_a}}\times \\ \times\int\limits_{\theta_0}^{\theta_m}\sqrt{\frac{(K_1\sin^2\theta + K_3\cos^2\theta)(\epsilon_\perp + \epsilon_a\cos^2\theta)}{\cos^2\theta - \cos^2\theta_m}}\,d\theta, \tag{7}$$

$$\frac{(K_1\sin^2\theta_0 + K_3\cos^2\theta_0)(\cos^2\theta_0 - \cos^2\theta_m)}{(\epsilon_\perp + \epsilon_a\cos^2\theta_m)(\epsilon_\perp + \epsilon_a\cos^2\theta_0)} = \\ = \frac{\pi}{\epsilon_\parallel\epsilon_\perp\epsilon_a E_0^2}\left(W_e\sin 2\theta_0 + W_\nu\sin 2(\theta_0 - \psi)\right)^2, \tag{8}$$

which can be solved only numerically.

In the absence of the external electric field ($E_0 = 0$), the solution of Eq. (4) with boundary conditions (5) is trivial and is given by the expression

$$\theta(z) = \theta_0 = \frac{1}{2}\arctan\frac{W_\nu\sin 2\psi}{W_e + W_\nu\cos 2\psi}, \tag{9}$$

where the value of arctan has to be reduced to the first quadrant. It is evident that the director angle in the cell bulk does not depend on the coordinate z and coincides with its value at the substrate surface. As a consequence, the director field is uniform.

Figures 2 and 3 illustrate the calculated dependences of the values of the director angle θ_0 at the cell surface and the maximum director angle θ_m in

the NLC bulk, respectively, on the magnitude of the external electric field strength E_0. The calculations were performed for the values of the dimensionless anchoring energies $w_e = W_e L/K_3 = 4$ and $w_\nu = W_\nu L/K_3 = 6$, the orientation angle of the easy axis ν $\psi = 1^\circ$, the cell thickness $L = 10$ μm, and the NLC parameter values $\epsilon_\parallel = 19$, $\epsilon_\perp = 5$, $K_1 = 1.1 \times 10^{-6}$ dyn, and $K_3 = 1.5 \times 10^{-6}$ dyn, which are close to typical ones [64]. In particular, the given values of the NLC parameters correspond to the widely used liquid crystal mixture Merck E7 [50, 65, 66].

As the results of calculations show, if the electric field strength E_0 increases from zero, the values of the director angles θ_0 and θ_m begin to grow continuously from their initial value (9). The loss of stability by the initial director state (9) has a non-threshold character provided that the director has a pretilt at the confining surface, and a threshold one in the absence of the pretilt [67]. Similarly to the case where the director pretilt at the surface is absent [67], if the electric field strength E_0 increases further, jump-like orientational transitions may arise in the system: first, from a homogeneously oriented state close to the homeotropic one into an inhomogeneous state, and afterwards from the inhomogeneous state into a weakly inhomogeneous one close to the planar state. These transitions have a threshold character and are accompanied by a hysteresis (see Figs. 2 and 3). In this case, when the strength E_0 reaches the critical value $E_{0\text{th}}$, the system jumps from a state close to the homogeneous one to a substantially heterogeneous state or vice versa. Note that if the voltage is reduced, inverse transitions also have the threshold character, but they occur at lower critical strengths of the electric field than in the case of the strength growing, $E_{0\text{th}} < E_{0\text{th}}$. In general, two hystereses of orientational transitions can be observed when the magnitude of the electric field strength in the system changes; namely, from the homeotropically and planarly oriented states into an inhomogeneous one.

The stationary solutions for which $\partial\theta/\partial E_0 < 0$ (see Figs. 2 and 3) are unstable with respect to small deformations of the director field, which can be shown in the following way. The temporal behavior of the director angle θ in the NLC bulk is determined by the modified equation (4) with the term $\eta_V \partial\theta/\partial t$ in the right-hand side, where $\eta_V > 0$ is the coefficient of NLC bulk viscosity. Let θ_1 and $\theta_2 = \theta_1 + \delta\theta$ be infinitely close stationary solutions corresponding to infinitely close values E_{01} and $E_{02} = E_{01} + dE_0$ of the electric field strength. Here, the small values $\delta\theta < 0$ and $dE_0 > 0$ correspond to the case $\partial\theta/\partial E_0 < 0$. Let us consider the evolution of the stationary solution θ_2 at the electric field strength E_{01}. Since $E_{02} > E_{01}$, it follows from the modified equation (4) that the derivative $\partial\theta/\partial t < 0$, i.e., the solution moves away with time from the stationary value θ_1. Thus, the solution θ_1 is unstable with respect to the small perturbation $\theta_1 \to \theta_1 + \delta\theta$. Therefore, the sections where the derivative $\partial\theta/\partial E_0 < 0$ (see Figs. 2 and 3) correspond to unstable stationary solutions.

If the external electric field strength increases and reaches the value $E_0 \approx 170$ V/mm (Fig. 2), the director deviation angle θ_0 at the surface and the maximum director angle θ_m in the NLC bulk increase in a jump-like manner by approximately $\Delta\theta_0 \approx 0.15\pi$ and $\Delta\theta_m \approx 0.45\pi$, respectively. The inverse transition occurs at a lower strength value, $E_0 \approx 120$ V/mm, and with smaller amplitudes of the jump-like director reorientation, namely, $\Delta\theta_0 \approx 0.1\pi$ and $\Delta\theta_m \approx 0.4\pi$, respectively.

At external electric field strengths of about 230 V/mm, the director reorientation is accompanied by another hysteresis located near the value $\theta(z) = \pi/2$. For typical values of the NLC cell parameters, this hysteresis is much smaller both in its width (the difference between the critical strength values for the direct and inverse transitions) and the amplitude $\Delta\theta_m$ of the change in the maximum director angle. However, the amplitudes of the director angle change $\Delta\theta_0$ at the surface are of the same order of magnitude for both hystereses.

In Fig. 4, the profiles of the director angle θ across the cell thickness are shown for various values of the external electric field strength within an interval from 100 to 250 V/mm. In electric fields with a strength below 160 V/mm, the values of the director angle θ are localized near its initial value (9), with the maximum deviation not exceeding $\Delta\theta \approx$ $\approx 0.02\pi$. If the electric field strength reaches $E_0 \approx$ ≈ 170 V/mm, the system jumps from a weakly inhomogeneous homeotropic state into a substantially inhomogeneous one. On this way, no smooth increase of the strength magnitude E_0 can bring about the values of the director angle within an interval from 0.02π to 0.18π. Further growth of the strength E_0 leads to a smooth increase of the director angle θ near the cell

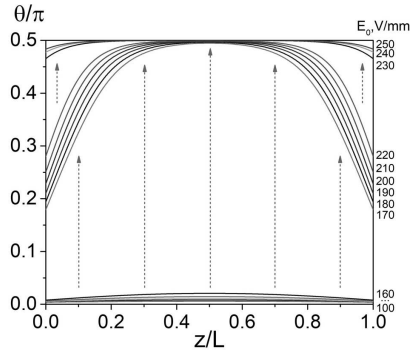

Fig. 4. Stationary profiles of the director angle θ across the cell thickness for increasing electric field strengths E_0. The arrows mark orientational transitions in the cell

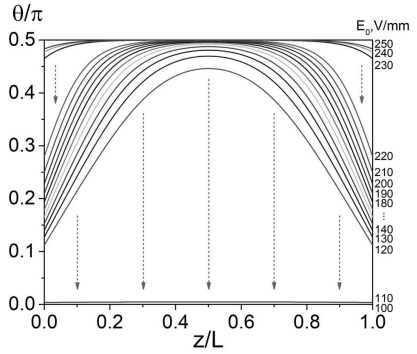

Fig. 5. Stationary profiles of the director angle θ across the cell thickness for decreasing electric field strengths E_0. The arrows mark orientational transitions in the cell

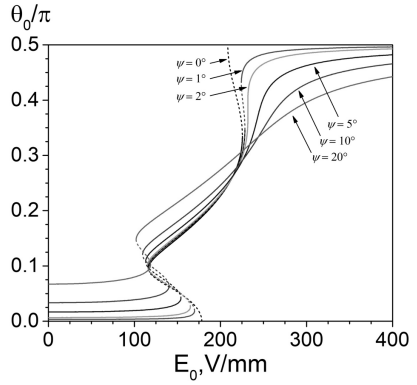

Fig. 6. Stationary dependences of the director angle θ_0 at the cell surface on the electric field strength E_0 for various orientation angles ψ of the easy axis ν

surfaces, $z/L \in [0, 0.3]$ and $z/L \in [0.7, 1]$. When the field strength reaches the critical value of the second hysteresis transition (about 230 V/mm), the director field undergoes a jump-like reorientation near the confining surfaces so that the system passes into a weakly inhomogeneous planar state. Note that, in the absence of the director pretilt at the cell surface, the planar state can be achieved, strictly speaking, only in the approximation $E_0 \to \infty$ [67].

If the electric field strength decreases from 250 to 100 V/mm (Fig. 5), the director field relaxes from a weakly inhomogeneous planar state [$\theta(z) \approx \pi/2$] into the initial homogeneous one (9). Note that the critical field strength values for the direct and inverse hysteresis transitions in the system from a weakly inhomogeneous planar state into a substantially inhomogeneous one and vice versa are close by magnitude(the width of the hysteresis loop is about 10 V/mm). Therefore, the values of the director angle θ that are realized, when the electric field strength diminishes within an interval of 170÷250 V/mm are close to those achieved when the field strength increases. However, the hysteresis loop width at the system transition from a substantially inhomogeneous state to the initial weakly inhomogeneous homeotropic one and vice versa equals about 60 V/mm. Note that if the magnitude of the electric field strength decreases below 170 V/mm, it becomes possible to reach the values of the director angle θ within an interval of $0.12\pi \div 0.18\pi$, which cannot be realized by increasing the field strength only.

An increase in the director pretilt at the substrate surface, which is provided by the orientation angle ψ of the easy axis ν, leads to the smoothing of the angular dependences $\theta_0(E_0)$ and $\theta_m(E_0)$ (see Fig. 6) and, as a result, to a reduction in the width and amplitude of both hysteresis transitions in the system. Already at the angle $\psi \approx 2°$, the hysteresis at the system transitions from an inhomogeneous state to a planar one and vice versa ($E_{0\text{th}} \approx 240$ V/mm) disappears. As the values of the angle ψ increase, the hysteresis at the system transitions from a homeotropic state into a non-homogeneous one and vice versa shifts towards lower critical strength values.

According to the results of calculations, irrespective of the type of orientational transition in the system, the interval of the hysteresis existence is determined not only by the magnitude of the electric field strength E_0 but also by the values of the anchoring energies w_e and w_ν, the parameter ratio K_1/K_3, and the magnitude of the orientation angle ψ of the easy axis ν. In Fig. 7, the numerically calculated dependences of the critical angle ψ_{th} on the anchoring en-

ergy w_ν of the director with the inclined easy axis ν are plotted for several values of the ratio K_1/K_3. One can see that a hysteresis accompanies the orientational transitions between the homeotropic and inhomogeneous states (in the interval $\psi < \psi_{\rm th1}$) and between the planar and inhomogeneous ones (in the interval $\psi < \psi_{\rm th2}$). At $\psi > \psi_{\rm th1}$ in the former case and $\psi > \psi_{\rm th2}$ in the latter one, the corresponding orientational transitions occur without the hysteresis. Regardless of the type of the orientational transition in the system, the reduction of the anchoring energy w_ν leads to an expansion of the hysteresis region in the magnitude of the angle ψ. It is obvious that at lower values of the coupling energy w_ν, larger values of the inclination angle ψ of the easy axis ν are needed in order to localize the influence of the easy axis $\mathbf{e}$ and destroy the hysteresis in the corresponding orientational transition. For large values of the anchoring energy, $w_\nu \gtrsim 6$, relatively small inclination angles ψ of the easy axis ν, $\psi \gtrsim 0.05\pi$, are sufficient for the hysteresis in the orientational transition of the system from the planar state into an inhomogeneous one to disappear. In this case, as the ratio K_1/K_3 decreases, the hysteresis region becomes narrower in the angle ψ.

Unlike the orientational transition of the system from the planar state to an inhomogeneous one, the hysteresis at the system transition from the homeotropic state into an inhomogeneous one survives in a much wider interval of the inclination angle ψ of the easy axis ν. In this case, as the value of the ratio K_1/K_3 increases, the critical values $\psi_{\rm th1}$ decrease monotonically at the anchoring energies $w_\nu \gtrsim \gtrsim 8$ and change non-monotonically otherwise.

Note that the angle interval $\psi < \psi_{\rm th2}$ is a region of a "double" hysteresis. In the angle interval $\psi_{\rm th2} < \psi < \psi_{\rm th1}$, there is only one hysteresis, namely, corresponding to the orientational transition of the system from the homeotropic state to an inhomogeneous one.

In general, the growth of the anchoring energy w_ν and the orientation angle ψ of the easy axis ν leads to the narrowing of the hysteresis loop and its subsequent disappearance at both orientational transitions. At the same time, the increase of the ratio K_1/K_3 leads to an expansion of the range of change of the director angle θ at the hysteretic transition of the system from the planar state into an inhomogeneous one or to its narrowing in the case of the hysteretic transition of the system from the homeotropic state into a heterogeneous one, which is in agreement with the results of work [67].

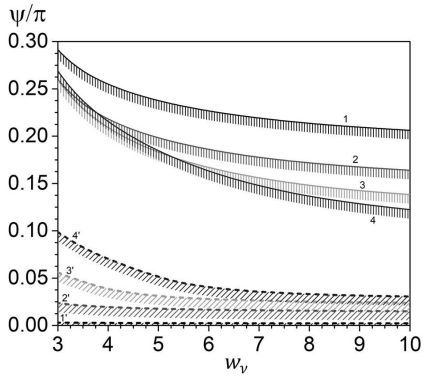

Fig. 7. Dependences of the critical values $\psi_{\rm th1,2}$ on the anchoring energy $w_\nu = W_\nu L/K_3$ for $K_3 = 1.5 \times 10^{-6}$ dyn, $w_e = W_e L/K_3 = 2$, and various values of the ratio $K_1/K_3 = 0.5$ (*1*, *1′*), 1 (*2*, *2′*), 1.5 (*3*, *3′*), and 2 (*4*, *4′*): $\psi_{\rm th1}$ (solid curves), $\psi_{\rm th2}$ (dashed curves). The hatching marks the hysteresis intervals of orientational transition

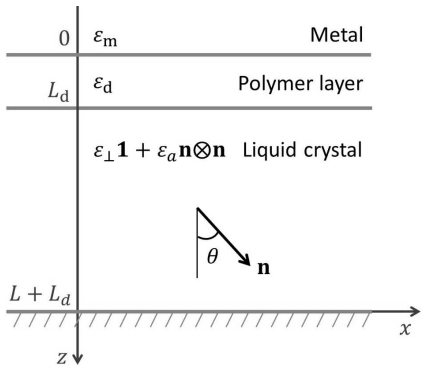

Fig. 8. Geometry of the liquid crystal–polymer layer–metal structure. Surface plasmon polaritons (SPPs) can propagate at the polymer layer–metal interface

3. Plasmon Oscillations at the NLC Cell Surface

Let the outer side of one of the cell substrates (this is a thin polymer layer of thickness L_d) be in contact with a metal layer, for example, gold. Then, under suitable conditions, surface plasmon polaritons (SPPs) can be excited at the interface between the polymer layer and the metal. Let us consider the propagation of SPPs in this system along the Ox-axis (see Fig. 8). The Oz-axis is directed towards the NLC, and the plane $z = 0$ coincides with the polymer–metal interface.

The electromagnetic field of the SPP is written in the form of a monochromatic wave of frequency ω,

$$\mathbf{E}(\mathbf{r},t)=\mathbf{E}(\mathbf{r})e^{-i\omega t},\quad \mathbf{H}(\mathbf{r},t)=\mathbf{H}(\mathbf{r})e^{-i\omega t}.$$

Since the SPP is a localized mode, the oscillation amplitudes of its electric and magnetic fields decay exponentially when moving away from the plane of this mode propagation. If the polymer layer is thin enough, then the SPP electromagnetic field, when penetrating the NLC, will perceive the director field orientation. Owing to the exponential decay of the SPP electromagnetic field, the influence of the substrate on the other side of the NLC cell ($z \geqslant L+L_d$) on the propagation parameters of this field is negligibly small. Therefore, in the framework of our consideration of the SPP electromagnetic field, the NLC will be assumed infinite in the direction of the Oz-axis. Hence, the medium, where the SPP propagates is simulated as a three-layer optical system consisting of an isotropic homogeneous polymer layer confined from both sides by semi-infinite metal and NLC layers.

To make allowance for the influence of the NLC anisotropy and heterogeneity on the SPP propagation, let us apply the perturbation theory [50, 67]. In the zeroth approximation of this theory, the strength vectors of the SPP electric, $\mathbf{E}(\mathbf{r})$, and magnetic, $\mathbf{H}(\mathbf{r})$, fields are sought as solutions of the system of Maxwell equations for a homogeneous isotropic medium with the dielectric permittivity

$$\varepsilon_0(z)=\varepsilon_m\chi(-z)+\varepsilon_d\chi(z), \tag{10}$$

where ε_m and ε_d are the dielectric constants of the metal and the polymer, respectively, at the SPP frequency ω; and $\chi(t)$ is the Heaviside function: $\chi(t)=0$ if $t<0$, and $\chi(t)=1$ if $t>0$. The solutions for the strength vectors of the SPP electric and magnetic fields in the zeroth approximation of the perturbation theory look like

$$\mathbf{E}_0^{m,d}(\mathbf{r})=\frac{cA_0}{\omega\varepsilon_{m,d}}\big(\pm i\beta_{m,d},0,-k_{0x}\big)e^{i\mathbf{k}_0^{m,d}\mathbf{r}}, \tag{11}$$

$$\mathbf{H}_0^{m,d}(\mathbf{r})=A_0\big(0,1,0\big)e^{i\mathbf{k}_0^{m,d}\mathbf{r}}, \tag{12}$$

where A_0 is an amplitude multiplier; and the subscripts m and d denote, respectively, the metal ($z<0$) and polymer ($z>0$) environments. The non-zero components of the wave vector $\mathbf{k}_0^{m,d}=(k_{0x},0,\pm i\beta_{m,d})$ are as follows:

$$k_{0x}=\frac{\omega}{c}\sqrt{\frac{\varepsilon_d\varepsilon_m}{\varepsilon_d+\varepsilon_m}},\quad \beta_{m,d}=\frac{\omega}{c}\sqrt{-\frac{\varepsilon_{m,d}^2}{\varepsilon_d+\varepsilon_m}}. \tag{13}$$

The next step is to account for the anisotropy and heterogeneity of the NLC as a perturbation of the zeroth-order solution. For this purpose, let us write down the dielectric constant of the considered structure in the form

$$\hat{\varepsilon}(z)=\varepsilon_0(z)\hat{\mathbf{1}}+\eta\Delta\hat{\varepsilon}(z), \tag{14}$$

where

$$\Delta\hat{\epsilon}(z)=\left[\varepsilon_a\left(\mathbf{n}\otimes\mathbf{n}-\mathbf{1}/3\right)+\varepsilon_c\mathbf{1}\right]\chi(z-L_d); \tag{15}$$

$\varepsilon_a=\varepsilon_\parallel-\varepsilon_\perp$; $\varepsilon_c=(2\varepsilon_\perp+\varepsilon_\parallel)/3-\varepsilon_d$; $\varepsilon_\parallel$ and $\varepsilon_\perp$ are the components of the dielectric permittivity tensor of the homogeneous NLC that are parallel and perpendicular, respectively, to the NLC director and calculated at the frequency ω; and $\eta\ll 1$.

Let us find the solution to the system of Maxwell equations in a medium with the dielectric constant tensor $\hat{\varepsilon}(z)$ [Eq. (14)]. To do this, let us expand the strength vectors of the SPP electric and magnetic fields in series in the small parameter η,

$$\mathbf{E}=\mathbf{E}_0+\eta\mathbf{E}_1+o(\eta), \tag{16}$$

$$\mathbf{H}=\mathbf{H}_0+\eta\mathbf{H}_1+o(\eta). \tag{17}$$

Here, the vectors $\mathbf{E}_0$ and $\mathbf{H}_0$ correspond to solutions (11) and (12) found above for the zeroth order perturbation in the isotropic approximation, and the corrections $\mathbf{E}_1$ and $\mathbf{H}_1$ take into account the presence of the NLC layer. By solving the equations for $\mathbf{E}_1$ and $\mathbf{H}_1$ in the linear approximation in η, we find a correction to the zeroth approximation $n_{\text{eff}}^0=ck_{0x}/\omega$ of the SPP effective refractive index. The corrected quantity takes the form

$$n_{\text{eff}}=n_{\text{eff}}^0+\frac{c}{\omega}\,k_{0x}\,Ke^{-2\beta_dL_d}, \tag{18}$$

where

$$K=\frac{\varepsilon_m\varepsilon_c}{2\left(\varepsilon_d+\varepsilon_m\right)\varepsilon_d}-\frac{\left(\varepsilon_d+2\varepsilon_m\right)\varepsilon_m\varepsilon_a}{6\varepsilon_d\left(\varepsilon_d^2-\varepsilon_m^2\right)}+$$
$$+\frac{\varepsilon_m\varepsilon_a}{2\varepsilon_d\left(\varepsilon_d-\varepsilon_m\right)}-\frac{\varepsilon_m\varepsilon_a\beta_de^{2\beta_dL_d}}{\varepsilon_d\left(\varepsilon_d-\varepsilon_m\right)}\times$$
$$\times\int_{L_d}^{\infty}\sin^2\theta(z-L_d)\,e^{-2\beta_dz}\,dz. \tag{19}$$

Expressions (18) and (19) allow the value of the SPP effective refractive index to be calculated for an arbitrary director profile in the NLC bulk.

In Fig. 9, the dependences of the SPP effective refractive index n_{eff} on the external electric field strength E_0 calculated for several wavelengths $\lambda = 2\pi c/\omega$ equal to 700, 800, and 900 nm are exhibited. The calculations were made for the following NLC cell parameters: $w_e = W_e L/K_3 = 2$, $w_\nu = W_\nu L/K_3 = 8$, $\psi = 1°$, $\epsilon_\parallel = 19$, $\epsilon_\perp = 5$, $K_1 = K_3 = 1.1 \times 10^{-6}$ dyn, $K_3 = 1.5 \times 10^{-6}$ dyn, $L = 10$ μm, and $L_d = 100$ nm. The optical frequency dependences of the dielectric constants of gold [51], polyvinylcarbazole [51] (as a polymer layer of the substrate), and the E7 mixture [68] (as the NLC) were taken into account. In particular, the following values were obtained for $\lambda = 800$ nm: $\varepsilon_m = -26.43$, $\varepsilon_d = 2.81$, $\varepsilon_c = -0.32$, and $\varepsilon_a = 0.64$.

In general, the growth of the electric field strength E_0 leads to a decrease in the values of the SPP effective refractive index n_{eff}. At the electric field strengths $E_0 \lesssim 170$ V/mm, the dependence of n_{eff} on E_0 is weak because the director field is a weakly deformed homeotropic structure. The interval of strength values 170÷230 V/mm is the region of the enhanced sensitivity of the quantity n_{eff} to the values of E_0. In particular, the increase of the E_0-values in the indicated interval is accompanied by a jump-like decrease of the n_{eff}-values, which is a direct consequence of the relevant jump-like reorientation of the director field. If the electric field strength exceeds a certain value close to 230 V/mm, the SPP effective refractive index practically ceases to depend on E_0-values because in this case the NLC director is oriented along the electric field almost everywhere across the cell thickness. If the strength E_0 decreases, the jump-like changes of the SPP parameter n_{eff} occur at lower strength values than in the case when it increases. As one can see, the changes of the n_{eff}-values induced by the changes of the electric field strength E_0 may be accompanied by hysteresis phenomena. These hystereses are a direct manifestation of the corresponding hystereses in the orientational rearrangement of the NLC director field. Similarly to the above-considered dependence of the director angle θ on the electric field strength E_0, the sections of the dependence $n_{\text{eff}}(E_0)$ where the derivative $\partial n_{\text{eff}}/\partial E_0 < 0$ correspond to unstable solutions (see Fig. 4). According to the calculation results, the increase of the wavelength λ leads to a reduction of the SPP effective refractive index n_{eff} and an expansion of the range of their variation.

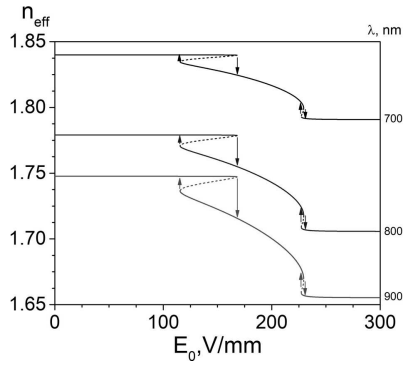

Fig. 9. Dependences of the SPP effective refractive index n_{eff} on the electric field strength E_0 for various values of the SPP wavelength λ

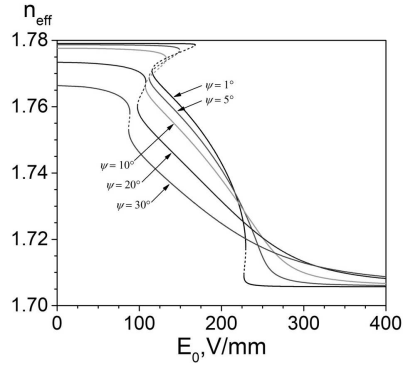

Fig. 10. Dependences of the SPP effective refractive index n_{eff} on the electric field strength E_0 for various values of the angle ψ

Figure 10 illustrates the dependences of the SPP effective refractive index n_{eff} on the electric field strength E_0 for various values of the inclination angle ψ of the easy axis ν. The increase of the angle ψ leads to the narrowing of the range of variation of n_{eff}-values (these variations are achieved by changing the electric field strength E_0) and to the narrowing of the hysteresis loops in the dependences $n_{\text{eff}}(E_0)$ (and their subsequent disappearance).

Since the dependence of the SPP effective refractive index n_{eff} on the electric field strength E_0 is a monotonically decreasing function, it is possible to find the range of variation of n_{eff}-values by accounting for the explicit expressions for the NLC director field in the limiting cases $E_0 = 0$ and $E_0 \to \infty$. In the former case, the director angle is determined by Eq. (9); in

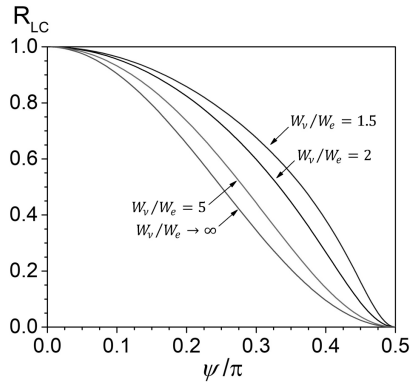

Fig. 11. Dependences of the multiplier R_{LC} in expression (20) for the control interval Δn_{eff} of the SPP effective refractive index on the inclination angle ψ of the axis **e** for various values of the ratio W_ν/W_e between the anchoring energies

the latter one, $\theta(z) \to \pi/2$, i.e., the director field is planar oriented. By substituting the indicated solutions into Eqs. (18) and (19), and using the explicit expressions for the components of the wave vector (13), we obtain an expression for the control interval of the SPP effective refractive index,

$$\Delta n_{\text{eff}} = R_\varepsilon R_{PL} R_{LC}, \tag{20}$$

where

$$R_\varepsilon = \sqrt{\frac{\varepsilon_d \varepsilon_m}{\varepsilon_d + \varepsilon_m}} \frac{|\varepsilon_m|\,\varepsilon_a}{\varepsilon_d\,(\varepsilon_d - \varepsilon_m)},$$
$$R_{PL} = \exp\left(-\frac{2\omega\varepsilon_d L_d}{c\,|\varepsilon_d + \varepsilon_m|}\right), \tag{21}$$
$$R_{LC} = \cos^2\left(\frac{1}{2}\arctan\frac{W_\nu \sin 2\psi}{W_e + W_\nu \cos 2\psi}\right),$$

as in expression (9), the values of arctan are reduced to the first quadrant. As one can see from formula (20), the expression for the range of variation Δn_{eff} of the SPP effective refractive index n_{eff} is the product of three separate multipliers: the multiplier R_ε describes the contribution of the dielectric constants of the components of the NLC–polymer layer–metal structure. The multiplier R_{PL} takes into account the weakening of the SPP sensitivity to the NLC reorientation owing to the presence of the polymer layer, and the multiplier R_{LC} makes allowance for the influence of the orientation angle ψ of the easy axis ν and the anchoring energies W_e and W_ν on the interval of variation of the director angle θ in the NLC cell.

As one can see from expressions (20) and (21), the SPP propagation frequency ω is explicitly included in the expression for the control range Δn_{eff} of the SPP effective refractive index only as a component of the multiplier R_{PL}. A reduction of the frequency ω slows down the attenuation of the SPP field when moving away from the interface between the polymer layer and the metal, which, in turn, enhances the ability to govern the optical properties of SPP by reorienting the NLC. In the absence of the polymer layer ($L_d = 0$), the value of the SPP frequency ω affects the control interval Δn_{eff} only indirectly, namely, through the frequency dependences of the dielectric constants of the structural components. Expectedly the control interval Δn_{eff} expands as the polymer layer thickness L_d decreases and the NLC optical anisotropy ε_a increases.

The increase of the orientation angle ψ of the easy axis ν and the increase of the ratio W_ν/W_e between the energies of NLC anchoring with the ν- and **e**-axes, respectively, lead to the narrowing of the control interval Δn_{eff} of the values of the SPP effective refractive index (see Fig. 11). In the limiting case $\psi \to 0$, the dependence of the quantity Δn_{eff} on the ratio W_ν/W_e between the anchoring energies disappears because then the axes ν and **e** coincide. At $\psi \to \pi/2$ and provided $W_\nu > W_e$, the control interval of the quantity n_{eff} narrows down to zero because the director becomes aligned planarly across the entire cell thickness, irrespective of the electric field strength value E_0.

4. Discussion of Results and Conclusions

The electrically induced orientational instability of the NLC director in a homeotropically oriented cell with the director pretilt at its surface has been studied theoretically. It is found that if the strength E_0 of the external electric field increases from zero, the deformations of the director field in the NLC bulk increase continuously, i.e., there is a non-threshold orientational transition from the initial homogeneous, almost homeotropic state into an inhomogeneous one. Note that, in the absence of the director pretilt at the surface, the indicated orientational transition has a threshold character. Further increase of E_0 induces an orientational transition in the system from a weakly inhomogeneous homeotropic state into a substantially inhomogeneous one and a subsequent tran-

sition into an almost homogeneous planar state. Under certain conditions, the indicated orientational transitions can be accompanied by hysteresis phenomena. In this case, when the electric field strength E_0 reaches certain critical values $E_{0\text{th}}$, the orientational transitions of the director field occur in a jump-like manner. When the electric field strength E_0 decreases, the inverse orientational transitions also take place in a jump-like manner, but, at lower critical strength values, $E_{0\text{th}} < E_{0\text{th}}$.

The existence conditions for hystereses at orientational transitions, the parameter values of those hystereses, and their dependence on the electric field strength E_0 are determined. The existence of the critical values ψ_{th1} and ψ_{th2} (here, $\psi_{\text{th1}} > \psi_{\text{th2}}$) for the orientation angle ψ of the inclined easy axis is shown. Namely, the orientational transitions between a weakly inhomogeneous homeotropic state and a substantially inhomogeneous one, which occurs at $\psi < \psi_{\text{th1}}$, and between a weakly inhomogeneous planar state and a substantially inhomogeneous one, which occurs at $\psi < \psi_{\text{th2}}$, are accompanied by the hysteresis phenomenon. As a result, the angle interval $\psi < \psi_{\text{th2}}$ is an interval of a "double" hysteresis, whereas both orientational transitions have no hysteresis at $\psi > \psi_{\text{th1}}$. The growth in the orientation angle ψ of the easy axis ν leads to a reduction of the hysteresis widths and amplitudes for both orientational transitions, their subsequent disappearance, and, as a result, the smoothing of the dependence $\theta(E_0)$ at all z-coordinate values. It is found that, for typical values of the NLC cell parameters, when the director pretilt angle ψ at the cell surface increases, the hysteresis of the orientational transition of the system from a weakly inhomogeneous planar state into a substantially inhomogeneous one disappears first. Further growth of the ψ-values leads also to the disappearance of the hysteresis in the orientational transition of the system from a weakly inhomogeneous homeotropic state into a substantially inhomogeneous one. With the increase of the anchoring energy W_ν of the director with the inclined easy axis, the ψ-angle intervals of the hysteresis existence of both orientational transitions become narrower. If the value of the ratio K_1/K_3 increases, the interval of existence of the hysteresis of the orientational transition in the system from a weakly inhomogeneous homeotropic state into a substantially inhomogeneous one broadens out; on the contrary, the interval of existence of the hysteresis of the orientational transition from a weakly inhomogeneous planar state into a substantially inhomogeneous one becomes narrower in this case.

The influence of the external electric field on the parameters and propagation conditions of plasmon polaritons at the surface of the NLC cell has been considered in the configuration that one of the polymer substrates of the cell is covered on the outer side by a thin layer of gold. The value of the SPP effective refractive index n_{eff} is calculated, and its dependences on the electric field strength E_0, the polymer layer thickness L_d, and the NLC cell parameters are analyzed. It is found that larger values of the electric field strength E_0 give rise to lower values of the SPP effective refractive index n_{eff}. The interval of variation Δn_{eff} of the SPP effective refractive index expands with the decrease of the orientation angle ψ of the inclined easy axis ν, the polymer layer thickness L_d, and the ratio W_ν/W_e between the anchoring energies, as well as with the growth of the SPP wavelength λ and the NLC optical anisotropy ε_a.

APPENDIX

Note that the integrand in formula (7) tends to $+\infty$ near the upper integration limit θ_m. This circumstance considerably complicates the process of calculating the corresponding integral numerically. This difficulty can be solved by representing the integrand as a sum of two terms,

$$\sqrt{\frac{(K_1 \sin^2\theta + K_3 \cos^2\theta)(\epsilon_\perp + \epsilon_a \cos^2\theta)}{\cos^2\theta - \cos^2\theta_m}} = A + B,$$

where

$$A = \sqrt{\frac{(K_1 \sin^2\theta_m + K_3 \cos^2\theta_m)(\epsilon_\perp + \epsilon_a \cos^2\theta_m)}{\sin 2\theta_m(\theta_m - \theta)}}$$

and

$$B = \sqrt{\frac{(K_1 \sin^2\theta + K_3 \cos^2\theta)(\epsilon_\perp + \epsilon_a \cos^2\theta)}{\cos^2\theta - \cos^2\theta_m}} - \\ - \sqrt{\frac{(K_1 \sin^2\theta_m + K_3 \cos^2\theta_m)(\epsilon_\perp + \epsilon_a \cos^2\theta_m)}{\sin 2\theta_m(\theta_m - \theta)}}.$$

Then, the singularity of the integrand in formula (7) becomes isolated in the term A, which admits the analytical integration,

$$\int_{\theta_0}^{\theta_m} A\, d\theta = 2\sqrt{(K_1 \sin^2\theta_m + K_3 \cos^2\theta_m)} \times \\ \times \sqrt{\frac{(\epsilon_\perp + \epsilon_a \cos^2\theta_m)(\theta_m - \theta_0)}{\sin 2\theta_m}}.$$

At the same time, the term B is a finite function of θ, without singular points, vanishes at $\theta \to \theta_m$, and can be integrated using numerical methods.

1. I.-C. Khoo. *Liquid Crystals* (John Wiley and Sons, 2022) [ISBN: 978-1-119-70582-6].
2. T. Kato, J. Uchida, T. Ichikawa, T. Sakamoto. Functional liquid crystals towards the next generation of materials. *Angew. Chem. Int. Edit.* **57**, 4355 (2018).
3. S. Sato. Applications of liquid crystals to variable-focusing lenses. *Opt. Rev.* **6**, 471 (1999).
4. M. Schadt. Liquid crystal materials and liquid crystal displays. *Annu. Rev. Mater. Sci.* **27**, 305 (1997).
5. P.-G. De Gennes, J. Prost. *The Physics Of Liquid Crystals* (Oxford University Press, 1993) [ISBN: 9780198517856].
6. J. P. Lagerwall, G. Scalia. A new era for liquid crystal research: Applications of liquid crystals in soft matter nano-, bio-, and microtechnology. *Curr. Appl. Phys.* **12**, 1387 (2012).
7. J. A. Castellano. Surface anchoring of liquid crystal molecules on various substrates. *Mol. Cryst. Liq. Cryst.* **94**, 33 (1983).
8. I. Yakovkin, A. Lesiuk, M. Ledney, V. Reshetnyak. Director orientational instability in a planar flexoelectric nematic cell with easy axis gliding. *J. Mol. Liq.* **363**, 119888 (2022).
9. O. Tarnavskyy, M. Ledney. Orientational instability of the director in a nematic cell caused by electro-induced anchoring modification. *Condens. Matter Phys.* **24**, 13601 (2021).
10. A. Ellison, I. A. Cornejo. Glass substrates for liquid crystal displays. *Int. J. Appl. Glass Sci.* **1**, 87 (2010).
11. O. Tarnavskyy, A. Savchenko, M. Ledney. Two-dimensional director configurations in a nematic-filled cylindrical capillary with the hybrid director alignment on its surface. *Liq. Cryst.* **47**, 851 (2020).
12. O. Tarnavskyy, M. Ledney. Equilibrium locations of defects in two-dimensional configurations of the nlc director field. *Liq. Cryst.* **50**, 21 (2023).
13. A. Lesiuk, M. Ledney, O. Tarnavskyy. Orientational instability of nematic liquid crystal in a homeotropic cell with boundary conditions controlled by an electric field. *Liq. Cryst.* **46**, 469 (2019).
14. A. Lesiuk, M. Ledney, O. Tarnavskyy. Orientational instability induced by the electric field in a cell of a nematic liquid crystal with negative dielectric anisotropy. *Ukr. J. Phys.* **62**, 779 (2017).
15. B.Y. Zel'dovich, N. Tabiryan, Y. S. Chilingaryan. Freedericksz transitions induced by light fields. *Sov. Phys. JETP* **54**, 32 (1981).
16. S. Durbin, S. Arakelian, Y. Shen. Optical-field-induced birefringence and freedericksz transition in a nematic liquid crystal. *Phys. Rev. Lett.* **47**, 1411 (1981).
17. A. Zolot'ko, V. Kitaeva, N. Kroo, N. Sobolev, L. Chillag. The effect of an optical field on the nematic phase of the liquid crystal ocbp. *JETP Lett.* **32**, 158 (1980).
18. E. Brasselet, A. Lherbier, L.J. Dubé. Transverse nonlocal effects in optical reorientation of nematic liquid crystals. *J. Opt. Soc. Am. B* **23**, 36 (2006).
19. M. Ledney, I. Pinkevych. Influence of anchoring at a nematic cell surface on threshold spatially periodic reorientation of a director. *Liq. Cryst.* **34**, 577 (2007).
20. A. Lesiuk, M. Ledney, O. Tarnavskyy *et al.* Electro-optical effect in a planar nematic cell with electric field sensitive boundary conditions. *Mol. Cryst. Liq. Cryst.* **647**, 320 (2017).
21. U. A. Laudyn, A. E. Miroshnichenko, W. Krolikowski *et al.* Observation of light-induced reorientational effects in periodic structures with planar nematic-liquid-crystal defects. *Appl. Phys. Lett.* **92**, 203304 (2008).
22. A.E. Miroshnichenko, E. Brasselet, Y.S. Kivshar. Light-induced orientational effects in periodic photonic structures with pure and dye-doped nematic liquid crystal defects. *Phys. Rev. A* **78**, 053823 (2008).
23. M. Ledney, O. Tarnavskyy, A. Lesiuk, V.Y. Reshetnyak. Interaction of electromagnetic waves in nematic waveguide. *Mol. Cryst. Liq. Cryst.* **638**, 1 (2016).
24. G. Barbero, N. Madhusudana, G. Durand. Weak anchoring energy and pretilt of a nematic liquid crystal. *J. Phys. Lett.–Paris* **45**, 613 (1984).
25. K.-W. Lee, A. Lien, J.H.S. Paek. Control and modification of nematic liquid crystal pretilt angles on polyimides. *Jpn. J. Appl. Phys.* **36**, 3591 (1997).
26. B. Cerrolaza, M.A. Geday, J. Oton, X. Quintana, N. Bennis. Measuring thickness and pretilt in reflective vertically aligned nematic liquid crystal displays. *Mol. Cryst. Liq. Cryst.* **494**, 222 (2008).
27. D. Seo, H. Matsuda, T. Oh-Ide, S. Kobayashi. Alignment of nematic liquid crystal (5cb) on the treated substrates: Characterization of orientation films, generation of pretilt angles, and surface anchoring strength. *Mol. Cryst. Liq. Cryst. A* **224**, 13 (1993).
28. F. K. Lee, B. Zhang, P. Sheng, H.S. Kwok, O.K. Tsui. Continuous liquid crystal pretilt control through textured substrates. *Appl. Phys. Lett.* **85**, 5556 (2004).
29. W.-T. Wu. *Liquid Crystal Pretilt Angle Control. Mechanism, Electro-Optical Properties and Numerical Analysis. Ph.D. thesis* (2016) [ISBN: 9789402804348].
30. L. Weng, P.-C. Liao, C.-C. Lin *et al.* Anchoring energy enhancement and pretilt angle control of liquid crystal alignment on polymerized surfaces. *AIP Adv.* **5**, 097218 (2015).
31. X. Nie, R. Lu, H. Xianyu, T.X. Wu, S.-T. Wu. Anchoring energy and cell gap effects on liquid crystal response time. *J. Appl. Phys.* **101**, 103110 (2007).
32. X. Nie, H. Xianyu, R. Lu, T.X. Wu, S.-T. Wu. Pretilt angle effects on liquid crystal response time. *J. Displ. Technol.* **3**, 280 (2007).
33. H.L. Ong. Optically induced Freedericksz transition and bistability in a nematic liquid crystal. *Phys. Rev. A* **28**, 2393 (1983).
34. A. Vella, B. Piccirillo, E. Santamato. Coupled-mode approach to the nonlinear dynamics induced by an elliptically

polarized laser field in liquid crystals at normal incidence. *Phys. Rev. E* **65**, 031706 (2002).
35. E. Brasselet, B. Piccirillo, E. Santamato. Three-dimensional model for light-induced chaotic rotations in liquid crystals under spin and orbital angular momentum transfer processes. *Phys. Rev. E* **78**, 031703 (2008).
36. I. Budagovsky, D. Pavlov, S. Shvetsov *et al.* First-order light-induced orientation transition in nematic liquid crystal in the presence of low-frequency electric field. *Appl. Phys. Lett.* **101**, 021112-1 (2012).
37. G. D'Alessandro, A. A. Wheeler. Bistability of liquid crystal microcavities. *Phys. Rev. A* **67**, 023816 (2003).
38. V. Ilyina, S. Cox, T. Sluckin. A computational approach to the optical freedericksz transition. *Opt. Commun.* **260**, 474 (2006).
39. M. F. Ledney, O S. Tarnavskyy. Influence of the anchoring energy on hysteresis at the freedericksz transition in confined light beams in a nematic cell. *Liq. Cryst.* **39**, 1482 (2012).
40. M. Ledney, O. Tarnavskyy, V. Khimich. Influence of dc electric field on the hysteresis of light-induced Freedericksz transition in a nematic cell. *Ukr. J. Phys.* **61**, 117 (2016).
41. B. Frisken, P. Palffy-Muhoray. Electric-field-induced twist and bend freedericksz transitions in nematic liquid crystals. *Phys. Rev. A* **39**, 1513 (1989).
42. I.W. Stewart, *The Static And Dynamic Continuum Theory Of Liquid Crystals: A Mathematical Introduction*, (CRC Press, 2019).
43. H. Zhou, E.P. Choate, H. Wang. Optical fredericks transition in a nematic liquid crystal layer. In *Liquid Crystalline Polymers: Volume 2–Processing and Applications*(Springer, 2015), p. 265.
44. G. Sprokel, R. Santo, J. Swalen. Determination of the surface tilt angle by attenuated total reflection. *Mol. Cryst. Liq. Cryst.* **68**, 29 (1981).
45. G. Sprokel. The reflectivity of a liquid crystal cell in a surface plasmon experiment. *Mol. Cryst. Liq. Cryst.* **68**, 39 (1981).
46. K. Welford, J. Sambles. Detection of surface director reorientation in a nematic liquid crystal. *Appl. Phys. lett.* **50**, 871 (1987).
47. K. Welford, J. Sambles, M. Clark. Guided modes and surface plasmon-polaritons observed with a nematic liquid crystal using attenuated total reflection. *Liq. Cryst.* **2**, 91 (1987).
48. A. Lesiuk, M. Ledney, V.Y. Reshetnyak. Light-induced fredericks transition in the nematic liquid crystal cell with plasmonic nanoparticles at a cell bounding substrate. *Phys. Rev. E* **106**, 024706 (2022).
49. K.R. Daly. *Light–Matter Interaction In Liquid Crystal Cells*. Ph.D. thesis (University of Southampton, 2011).
50. K.R. Daly, S. Abbott, G. D'Alessandro, D.C. Smith, M. Kaczmarek. Theory of hybrid photorefractive plasmonic liquid crystal cells. *J. Opt. Soc. Am. B* **28**, 1874 (2011).
51. S. B. Abbott. *Energy Transfer Between Surface Plasmon Polariton Modes With Hybrid Photorefractive Liquid Crystal Cells*. Ph.D. thesis (University of Southampton, 2012).
52. S. B. Abbott, K. R. Daly, G. D'Alessandro, M. Kaczmarek, D. C. Smith. Photorefractive control of surface plasmon polaritons in a hybrid liquid crystal cell. *Opt. Lett.* **37**, 2436 (2012).
53. M.E. Caldwell, E.M. Yeatman. Surface-plasmon spatial light modulators based on liquid crystal. *Appl. Opt.* **31**, 3880 (1992).
54. U. Bortolozzo, S. Residori, J. Huignard. Beam coupling in photorefractive liquid crystal light valves. *J. Phys. D* **41**, 224007 (2008).
55. F. Yang, J. Sambles. Microwave liquid crystal wavelength selector. *Appl. Phys. Lett.* **79**, 3717 (2001).
56. Y. Wang. Voltage-induced color-selective absorption with surface plasmons. *Appl. Phys. Lett.* **67**, 2759 (1995).
57. Y. Wang, S.D. Russell, R.L. Shimabukuro. Voltage-induced broad-spectrum reflectivity change with surface-plasmon waves. *J. Appl. Phys.* **97**, 023708 (2005).
58. O. Buchnev, A. Dyadyusha, M. Kaczmarek, V. Reshetnyak, Y. Reznikov. Enhanced two-beam coupling in colloids of ferroelectric nanoparticles in liquid crystals. *J. Opt. Soc. Am. B* **24**, 1512 (2007).
59. G. Cook, A. Glushchenko, V. Reshetnyak *et al.* Nanoparticle doped organic-inorganic hybrid photorefractives. *Opt. Expr.* **16**, 4015 (2008).
60. W. Dickson, G.A. Wurtz, P.R. Evans, R.J. Pollard, A.V. Zayats. Electronically controlled surface plasmon dispersion and optical transmission through metallic hole arrays using liquid crystal. *Nano Lett.* **8**, 281 (2008).
61. L. Komitov, G. Barbero, I. Dahl, B. Helgee, N. Olsson. Controllable alignment of nematics by nanostructured polymeric layers. *Liq. Cryst.* **36**, 747 (2009).
62. E. Ouskova, Y. Reznikov, S. Shiyanovskii *et al.* Photo-orientation of liquid crystals due to light-induced desorption and adsorption of dye molecules on an aligning surface. *Phys. Rev. E* **64**, 051709 (2001).
63. A. Rapini, M. Papoular. Distorsion d'une lamelle nématique sous champ magnétique conditions d'ancrage aux parois. *J. Phys. Colloq.* **30**, C4 (1969).
64. L.M. Blinov, V.G. Chigrinov. *Electrooptic Effects In Liquid Crystal Materials* (Springer Science and Business Media, 2012).
65. *Springer Handbook Of Materials Data*. Edited by H. Warlimont, W. Martienssen (Springer, 2018).
66. P.C.-P. Chao, Y.-Y. Kao, C.-J. Hsu. A new negative liquid crystal lens with multiple ring electrodes in unequal widths. *IEEE Photon. J.* **4**, 250 (2012).
67. I. Yakovkin, M. Ledney. Electrically induced orientational instability of the director in a homeotropic nematic liquid crystal cell and its effect on surface plasmon oscillations. *Phase Transit.* **97**, 394 (2023).

68. V. Tkachenko, G. Abbate, A. Marino *et al.* Nematic liquid crystal optical dispersion in the visible-near infrared range. *Mol. Cryst. Liq. Cryst.* **454**, 263 (2006).

Received 04.04.24.
Translated from Ukrainian by O.I. Voitenko

І.І. Яковкін, М.Ф. Ледней

ЕЛЕКТРОКЕРУВАННЯ
ПОВЕРХНЕВИМИ ПЛАЗМОННИМИ
КОЛИВАННЯМИ В ГОМЕОТРОПНІЙ
КОМІРЦІ НЕМАТИЧНОГО РІДКОГО КРИСТАЛА

Теоретично вивчається індукована електричним полем орієнтаційна нестійкість директора в комірці гомеотропно орієнтованого нематичного рідкого кристала (НРК) за наявності переднахилу директора на поверхні підкладинки. Встановлено, що орієнтаційні переходи поля директора НРК з вихідного однорідного стану в суттєво неоднорідний з наступним переходом в планарний стан, зумовлені зміною величини напруженості електричного поля, можуть супроводжуватися гістерезисами. За наявності останніх розраховано значення їх параметрів і встановлено області їх існування в залежності від величин параметрів НРК-комірки. Встановлено, що збільшення переднахилу директора на поверхні та зростання енергії зчеплення НРК з похилою легкою віссю приводять до звуження ширини петлі гістерезису, а в подальшому і до зникнення гістерезису зазначених орієнтаційних переходів. Досліджено поширення плазмонного поляритона на поверхні комірки НРК у випадку обмеженості однієї з її полімерних підкладинок з іншого боку шаром золота. Розраховано величину ефективного показника заломлення поверхневого плазмонного поляритона (ППП) та встановлено, що вона зменшується зі збільшенням напруженості електричного поля. Встановлено, що діапазон керування величиною ефективного показника заломлення ППП розширюється зі зменшенням значень кута орієнтування похилої легкої осі та товщини полімерного шару, а також зі збільшенням довжини хвилі ППП та оптичної анізотропії НРК.

Ключові слова: нематичний рідкий кристал, орієнтаційна нестійкість, гістерезис орієнтаційного переходу, переднахил директора, енергія зчеплення, поверхневий плазмонний поляритон.